



Published in final edited form as:

AAPS J. 2016 July ; 18(4): 898–913. doi:10.1208/s12248-016-9888-z.

## Multi-Functional Diarylurea Small Molecule Inhibitors of TRPV1 with Therapeutic Potential for Neuroinflammation

Zhiwei Feng<sup>1,2,3</sup>, Larry V. Pearce<sup>5</sup>, Yu Zhang<sup>1,2,3</sup>, Changrui Xing<sup>1,2,3</sup>, Brienna K. A. Herold<sup>5</sup>, Shifan Ma<sup>1,2,3</sup>, Ziheng Hu<sup>1,2,3</sup>, Noe A. Turcios<sup>5</sup>, Peng Yang<sup>1,2,3</sup>, Qin Tong<sup>1,2,3</sup>, Anna K. McCall<sup>5</sup>, Peter M. Blumberg<sup>5,6,7</sup>, and Xiang-Qun Xie<sup>1,2,3,4,7</sup>

<sup>1</sup>Department of Pharmaceutical Sciences and Computational Chemical Genomics Screening Center, School of Pharmacy, University of Pittsburgh, Pittsburgh, Pennsylvania 15261, USA

<sup>2</sup>NIDA National Center of Excellence for Computational Drug Abuse Research, University of Pittsburgh, Pittsburgh, Pennsylvania 15261, USA

<sup>3</sup>Drug Discovery Institute, University of Pittsburgh, Pittsburgh, Pennsylvania 15261, USA

<sup>4</sup>Departments of Computational Biology and of Structural Biology, University of Pittsburgh, Pittsburgh, Pennsylvania 15261, USA

<sup>5</sup>Laboratory of Cancer Biology and Genetics, National Cancer Institute, Bethesda, Maryland 20892, USA

<sup>6</sup>Laboratory of Cancer Biology and Genetics, National Institutes of Health, Building 37, Room 4048B, 37 Convent Drive MSC 4255, Bethesda, Maryland 20892-4255, USA

### Abstract

Transient receptor potential vanilloid type 1 (TRPV1), a heat-sensitive calcium channel protein, contributes to inflammation as well as to acute and persistent pain. Since TRPV1 occupies a central position in pathways of neuronal inflammatory signaling, it represents a highly attractive potential therapeutic target for neuroinflammation. In the present work, we have *in silico* identified a series of diarylurea analogues for hTRPV1, of which 11 compounds showed activity in the nanomolar to micromolar range as validated by *in vitro* biological assays. Then, we utilized molecular docking to explore the detailed interactions between TRPV1 and the compounds to

<sup>7</sup>To whom correspondence should be addressed. (xix15@pitt.edu; blumberp@dc37a.nci.nih.gov).

**Electronic supplementary material** The online version of this article (doi:10.1208/s12248-016-9888-z) contains supplementary material, which is available to authorized users.

### ASSOCIATED CONTENT

#### Supporting Information

Figure S1 shows the binding poses of capsaicin and RTX in our model. Figure S2 shows the inhibition of [<sup>3</sup>H]RTX binding to hTRPV1 by compound 14 with a  $K_i$  value of  $0.65 \pm 0.26$   $\mu$ M. Figure S3 shows the correlation between the predicted  $\Delta G$  of the binding and the  $\Delta G$  calculated from the experimental activities of 11 compounds. Figure S4 shows the distances between compound 4/5 and Phe543/Leu663 during 50 ns MD simulation. Figure S5 shows the comparisons of pore radius and conformational changes of hTRPV1 upon binding with compound 4 and with compound 5. Figure S6 shows compounds 14/16 bound to CB2 with modest potency ( $K_i=15.9/12.2$   $\mu$ M). Figure S7 shows the correlation between the number of hit compounds identified and the number of compounds screened in a 1000-compound data set using the CXCR2 model. Table S1 shows the structures of additional diarylurea small molecules found to have little or no measurable activity on hTRPV1 in the present work. Table S2 shows the experimental assay data for the compounds in the present work. See the supplemental material for more information.

### COMPLIANCE WITH ETHICAL STANDARDS

**Conflict of Interests** X.Q.X is a consultant for Oxis Biotech. The remaining authors declare no competing financial interests.

understand the contributions of the different substituent groups. Tyr511, Leu518, Leu547, Thr550, Asn551, Arg557, and Leu670 were important for the recognition of the small molecules by TRPV1. A hydrophobic group in R2 or a polar/hydrophilic group in R1 contributed significantly to the activities of the antagonists at TRPV1. In addition, the subtle different binding pose of *meta*-chloro in place of *para*-fluoro in the R2 group converted antagonism into partial agonism, as was predicted by our short-term molecular dynamics (MD) simulation and validated by bioassay. Importantly, compound 15, one of our best TRPV1 inhibitors, also showed potential binding affinity (1.39  $\mu$ M) at cannabinoid receptor 2 (CB2), which is another attractive target for immune-inflammation diseases. Furthermore, compound 1 and its diarylurea analogues were predicted to target the C-X-C chemokine receptor 2 (CXCR2), although bioassay validation of CXCR2 with these compounds still needs to be performed. This prediction from the modeling is of interest, since CXCR2 is also a potential therapeutic target for chronic inflammatory diseases. Our findings provide novel strategies to develop a small molecule inhibitor to simultaneously target two or more inflammation-related proteins for the treatment of a wide range of inflammatory disorders including neuroinflammation and neurodegenerative diseases with potential synergistic effect.

### Keywords

multi-targets; neuroinflammation; pain; synergistic effect; TRPV1

## INTRODUCTION

Neuroinflammation, which was once considered unlikely to occur due to the immune privileged characteristics of the nervous system, has recently emerged as a critical mechanism behind neurodegeneration. Its role is both positive and negative. In acute situations, short-term neuroinflammation is essential for recovery by limiting injury and facilitating healing; whereas in chronic and severe situations, neuroinflammation compromises host tissues and accelerates the neurodegenerative processes in the central nervous system (CNS) [1–3]. Various elements, such as protein aggregates, accumulation of abnormally modified cellular constituents, molecules from injured neurons or synapses, and dysregulation of inflammatory control mechanisms can provoke disordered neuroinflammation [3, 4]. Research into neurodegenerative diseases has shown that neuroinflammation contributes to the progress of many common degenerative disorders of the brain, such as Alzheimer's disease (AD), Parkinson's disease (PD), and Huntington's disease (HD) [5–8]. For example, amyloid beta(A $\beta$ )42 can give rise to neuroinflammation and further the neurodegenerative process [9]. Therefore, understanding and targeting neuroinflammation, the interface between the central nervous system and the immune system, could be a key strategy for future clinical therapies of neurodegenerative diseases.

Transient receptor potential vanilloid 1 (TRPV1) [10–14], a heat-sensitive and nonselective calcium-permeable cation channel of the TRP channel super-family, is a hub in the neuronal inflammatory signaling pathway network. TRPV1 has been reported to possess pro-inflammatory and nociceptive properties in the peripheral nervous system (PNS) and to contribute to acute and chronic pain [15], such as in osteoarthritis, neuropathic pain, migraine, inflammatory bowel disease, and bone cancer [16]. It is reported to be involved in

pain processing and modulation, thermoregulation, and neurogenesis [17]. TRPV1 has also been shown to be present in the brain and involved in synaptic plasticity and various other CNS functions. TRPV1 plays a pathogenic role in diverse neurological disorders ranging from PD [18] and AD [19] to anxiety, depression, and other mood disorders [20, 21]. One study showed that the TRPV1 agonist capsaicin could induce mesencephalic dopaminergic (MDA) neuron cell death, whereas the TRPV1 antagonists capsazepine and iodoresiniferatoxin could inhibit such neurotoxicity [22]. Given the associations among TRPV1, neuroinflammation and neurodegeneration, targeting TRPV1 represents not only a strategy for pain treatment but also a potential novel therapy for neurodegenerative disorders.

The recent release of *Rattus norvegicus* TRPV1 structures has significantly accelerated studies of the TRP channel family. In 2013, Julius and colleagues reported the structures of *R. norvegicus* apo-TRPV1 (rTRPV1) and of rTRPV1 bound with RTX/DkTx or with capsaicin, as determined by single particle electron cryo-microscopy [23]. In our previous work, we used the cryo-EM-derived structure of rTRPV1 to construct a 3D homology tetramer model of hTRPV1 exploiting this new level of structural understanding. The predicted binding pocket of hTRPV1 in our model was congruent with the experimental data and the cryo-EM structures of rTRPV1 [23]. The binding pocket was formed by Tyr511, Leu518, Leu547, Thr550, Arg557, Glu570, and Leu670. A five-point pharmacophore model derived from known antagonists was used to model and predict new antagonists for hTRPV1. Some of the virtual hits were identified and validated experimentally as the antagonists for hTRPV1.

In this work, we screened a series of new compounds which all contained as a core structure the diarylurea pharmacophore, and we identified a number of compounds with excellent TRPV1 activities ( $K_i$  as low as 470 nM) as validated by biological assays. Molecular docking and molecular dynamics (MD) simulation were used to generate insight into the different activities among compounds. We demonstrated that one of our most potent antagonists for TRPV1, compound 15, exhibited cannabinoid receptor 2 (CB2) inhibitory effect. In addition, the TRPV1 antagonist compound 1 was predicted to target the C-X-C chemokine receptor 2 (CXCR2), although this prediction still needs to be validated by bioassay. These results support the potential of modeling to identify anti-inflammatory compounds with a synergistic effect as a consequence of their being active at two independent therapeutic targets.

## MATERIALS AND METHODS

### Homology Model of hTRPV1

We used our previous homology model of human TRPV1 (hTRPV1) for further studies. Briefly, this model was constructed according to the cryo-EM-derived structure [23] of *R. norvegicus* TRPV1 (rTRPV1)-capsaicin (PDB entry: 3J5R, EM resolution: 4.2 Å). The 3D TRPV1 structural model has been previously validated by our MD simulations and bioassay data [24].

## Substructure Search of Diarylurea Small Molecules Targeting hTRPV1

We then performed the substructure search of diarylurea (derived from compound 1) against the refined compound library of 15,672 compounds [24] to evaluate diarylurea small molecules as ligands for TRPV1. Surflex-Sim with default parameters in SYBYL was used to perform the flexible aligning of ligands with the template (diarylurea). Thirty out of the top 50 compounds with a score higher than 7.0 were selected and purchased from either NCI or from commercial sources.

## Molecular Docking for the Studies of Ligand/hTRPV1 Interaction

Surflex-Dock GeomX (SFXC), a docking program in SYBYL, was used to generate the detailed ligand-receptor interactions, in which the docking score was expressed as  $-\log_{10}(K_d)$  [25]. The following parameters of docking were used in the present work: the additional starting conformation per molecule was set to 10, angstroms to expand search grid was set to 6, max conformation per fragment was set to 20, max number of rotatable bonds per molecule was set to 100, and the max number of poses per ligand was set to 100. The following flags were turned on: pre-dockminimization; post-dockminimization; molecule fragmentation; soft grid treatment; and activated spin alignment method with density of search was set to 3.0 and number of spins per alignment was set to 12. MMFF94S with MMFF94 charges [26] were used for the preparation of ligands. The binding poses displayed were selected from the cluster of poses obtained based on the frequency and on their docking score.

## Molecular Dynamics Simulation

After finishing the dockings, we chose structures of hTRPV1 bound with antagonist/partial agonist for performing the molecular dynamics (MD) simulations.

We paid special attention to the protonation states of His residues, in which His can be ionized at pH 7.40. VEGA ZZ software (version 2.4.0) [27] and PROPKA software (version 3.1) [28] were used to calculate the pK values of the protein. In the hTRPV1 model, all histidines were not protonated, due to the predicted pK values that were lower than 7.40 (from 2.52 to 6.85). Four residues were charged in the present work, including Asp-, Glu-, Lys+, and Arg+.

The VMD [29] program was used for embedding the protein-ligand complexes into a periodic and pre-equilibrated structure of 1-palmitoyl-2-oleoyl-sn-glycero-3-phosphatidylcholine (POPC). We eliminated the lipid molecules that were within 3 Å of the protein. Then, we inserted them into a TIP3P [30] water box and eliminated the waters molecules within 3 Å of the protein.

The systems (hTRPV1-compound 4/hTRPV1-compound 5, respectively) included the hTRPV1 model, 149/149 lipid molecules, 19434/19434 water molecules, 0/0 sodium ions, and 4/4 chloride ions for a total of 121448/121451 atoms per periodic cell. The sizes of the water-lipid box were  $110 \times 110 \times 110/110 \times 110 \times 110 \text{ \AA}^3$ . Then, two-step minimizations were conducted, in which each minimization was run for 50,000 steps. The first one was run

with the fixed protein, while the second one was run with flexible protein. 1.0 nanosecond (ns) MD of heating and equilibration were performed from 0°K to 310°K.

Treating the last frame of the equilibration as the starting point, we conducted 50 ns MD simulations by using the NAMD package [31] (version 2.9b1) with a CHARMM27 [32] force field within explicit water. Electrostatics were calculated by using the Particle Mesh Ewald [33] (PME) method, which was with a 12 Å non-bonded cutoff and a grid spacing of 1 Å per grid point in each dimension. The van der Waals energies were calculated by using two cutoff values. The switching radius was set to 10 Å. The cutoff radius was set to 12 Å. The temperature and pressure were maintained constant by a Langevin thermostat (310°K) and Langevin barostat (1 atm), respectively. The time step of the MD simulations was set to 1 femtosecond (fs). The data were saved every 10 pico-second (ps) for analysis. VMD software was used to analyze the trajectory from the MD simulation.

### TRPV1 Competition Binding Assay and Ca<sup>2+</sup> Uptake Assay

[<sup>3</sup>H]Resiniferatoxin ([<sup>3</sup>H]RTX, 37 Ci/mmol) and radioactive calcium (Ca<sup>2+</sup>, specific activity 5–30 Ci/g) were provided by PerkinElmer Life Sciences (Boston, MA). Non-radioactive RTX was obtained from LC Laboratories (Waltham, MA). Capsaicin was from Sigma-Aldrich (St. Louis, MO).

### Stable hTRPV1 Expression Cell Line Subculture

Conditions were as described previously [24]. Tet-On induced CHO-hTRPV1 cells were cultured in maintaining medium (F12 supplemented with 10% TET-free FBS (Atlanta Biologicals, GA), 25 mM HEPES, 10 µg/mL blasticidin and 250 µg/mL geneticin (all from Invitrogen Life Sciences; Grand Island, NY)). TRPV1 protein was induced with induction medium (F12 supplemented with 10% FBS, 25 mM HEPES, and 1 µg/mL tetracycline) as described below for ligand binding and Ca<sup>2+</sup> uptake measurements [34].

### RTX Competition Binding Assay

Binding studies with [<sup>3</sup>H]RTX were carried out as described previously [24]. Briefly, the binding assay mixtures were prepared in 1.5-mL centrifuge tubes and consisted of a fixed concentration (approximately 2 nM) of [<sup>3</sup>H]RTX (37 Ci/mmol specific activity, PerkinElmer Life Sciences), various concentrations of competing ligands, and 100 µg protein of membranes from induced CHO-hTRPV1-expressing cells (approximately 1–3 × 10<sup>6</sup> cells) in Dulbecco's phosphate-buffered saline (DPBS, with Ca<sup>2+</sup> and Mg<sup>2+</sup>) for a total volume of 350 µL. The assay mix contained bovine serum albumin at a final concentration of 0.25 mg/ml (Cohn fraction V; Sigma-Aldrich, St. Louis, MO). In each set of experiments, non-specific binding was determined in the presence of 200-nM non-radioactive RTX. The binding reaction was initiated by placing the assay mixture in a 37°C shaking water bath for 60 min (~30 rpm). The assay mixture was then chilled on ice for 2–3 min before adding 100 µL of α<sub>1</sub>-acid glycoprotein (2 mg/mL; Sigma-Aldrich) and mixed thoroughly. The tubes were kept on ice for an additional 10 min. The bound and free ligands were then separated by centrifugation (12,200 rpm for 15 min) in a Beckman Coulter centrifuge Allegra 21R. Two hundred microliters of supernatant were collected for determination of free ligand. The remainder was removed by aspiration. The bottom portion of the tubes containing the

membranes was cut off and bound radioactivity determined. Radioactivity was measured by scintillation counting. Data were analyzed using GraphPad Prism.  $K_i$  values for compounds were determined by competition for binding of [ $^3\text{H}$ ]RTX to the hTRPV1 and represent the mean  $\pm$ SEM of triplicate binding curves. In each curve, triplicate determinations were performed at each ligand concentration.

### Ca<sup>2+</sup> Uptake Assays

Assay conditions were as previously described [34]. CHO-hTRPV1 cells were plated in 24-well plates, reaching 40 to 60% confluence in maintaining medium after 24 h. The cells were washed once with Dulbecco's phosphate-buffered saline (DPBS; Invitrogen) to remove antibiotics, and fresh medium with tetracycline (inducing medium) was added to induce TRPV1 expression. Experiments were done approximately 24 h after induction. The cells were at least 90% confluent at the time of the assays [34].

For Ca<sup>2+</sup> uptake assays [34] testing agonists, the inducing medium was aspirated and replaced by DMEM supplemented with bovine serum albumin (BSA, 0.25 mg/mL), Ca<sup>2+</sup> (37 kBq/mL) and 100  $\mu\text{L}$  of increasing concentrations of the non-radioactive ligand for a total volume of 400  $\mu\text{L}$ /well. The cells were incubated for 5 min in a water bath at 37°C. For uptake measurements by a full agonist, a saturating concentration of capsaicin (3000 nM) was used as a positive control. Immediately after incubation, the assay medium was aspirated and the cells were washed twice with ice-cold DPBS (no Ca<sup>2+</sup> and Mg<sup>2+</sup>). The cells were then lysed in radioimmunoprecipitation assay buffer (50 mM Tris-Cl pH 7.5, 150 mM NaCl, 1% Triton X-100, 1% SDS, and 1% sodium deoxycholate; total volume of 400  $\mu\text{L}$ /well) for at least 40 min on a shaker. Aliquots (300  $\mu\text{L}$ ) of the cell lysates were counted in a liquid scintillation counter. Background uptake was determined in the absence of either compound or capsaicin. For the antagonism assays, capsaicin (30 nM) was included along with increasing concentrations of the ligand being evaluated. The cells were incubated for 5 min in a water bath at 37°C. Immediately after incubation, the assay medium was aspirated and the cells were washed twice with ice-cold DPBS (no Ca<sup>2+</sup> or Mg<sup>2+</sup>). The cells were then lysed in radioimmunoprecipitation assay buffer for at least 40 min on a shaker. Aliquots of the cell lysate were counted in a liquid scintillation counter. Triplicate points at each concentration of ligand were determined in each experiment. Compounds were initially screened in duplicate experiments at a concentration of 30  $\mu\text{M}$ . Compounds showing greater than 10% agonism/antagonism were evaluated in a third experiment at 30  $\mu\text{M}$  to provide a mean  $\pm$  SEM for the inhibition percentage. For all compounds that showed at least 50% inhibition at 30  $\mu\text{M}$  in these triplicate experiments, we then performed triplicate full-dose response curve measurements to obtain a mean  $\pm$  SEM for the  $K_i$ . Data were analyzed using GraphPad Prism.  $K_i$  values were calculated from the 50% inhibitory concentrations using the Chang-Prusoff equation [35]. For comparison, the cutoff of 50% inhibition at a 30- $\mu\text{M}$  concentration of antagonist corresponds approximately to an antagonist  $K_i$  of 14  $\mu\text{M}$  under our assay conditions.

### CB2 Radioligand Competition Binding Assay

The CB2 ligand competition binding assay was carried out as described previously [36, 37]. Briefly, non-radioactive ligands were diluted in binding buffer (50 mM Tris-Cl (pH 7.4), 5



mM MgCl<sub>2</sub>, 2.5 mM EGTA, and 0.1% (w/v) fatty acid-free BSA) supplemented with 10% dimethyl sulfoxide and 0.4% methyl cellulose. Each assay plate well contained a total of 200 μL of reaction mixture comprised of 5 μg of CB2 membrane protein, [<sup>3</sup>H]CP-55,940 ligand at a final concentration of 3 nM, and various concentrations of the unlabeled ligand. Plates were incubated at 30°C for 1 h with gentle shaking. The reaction was terminated by rapid filtration through Unifilter GF/B filter plates using a Unifilter Cell Harvester (PerkinElmer). After the plate was allowed to dry overnight, 30 μL MicroScint-0 cocktail (PerkinElmer) was added to each well and the radioactivity was counted by using a PerkinElmer TopCounter. All assays were performed in duplicate and data points represented as mean ± SEM.  $K_i$  values were determined from the bound radioactivity using non-linear regression analysis with GraphPad Prism. To determine control binding to CB2 in the absence of the competing ligand, binding of [<sup>3</sup>H]CP-55,940 to the membrane proteins was performed as described previously [38]. Briefly, the CB2 membrane fractions (5 μg) were incubated with increasing concentrations of [<sup>3</sup>H]CP-55,940 (0.05–4 nM) in 96-well plates at 30°C with slow shaking for 1 h. The binding buffer was supplemented with 10% dimethyl sulfoxide and 0.4% methylcellulose. Non-specific binding was determined in the presence of unlabeled CP-55,940 (5000 nM). The reaction was terminated and the radioactivity was counted as stated above. Non-linear regression analysis revealed the receptor density ( $B_{max}$ ) and the equilibrium dissociation constant ( $K_d$ ) values of [<sup>3</sup>H] CP-55,940 for the CB2 receptor.

## RESULTS

### Substructure Search of Diarylurea Small Molecules for TRPV1

We first docked capsaicin and RTX into our TRPV1 model, as shown in Figure S1 in the “Supporting Information” section. We found that both two agonists docked into the same pocket as did the other compounds in this work. These findings are also consistent with previous analyses. Although the cryo-EM of Julius *et al.* [23] could not reveal precisely how vanilloids bound, residues in close proximity can be observed. The EM map indicated the potential poses of RTX and capsaicin, which match with the binding pose of these two agonists in our hTRPV1 model. Our docking results were also congruent with the docking results of Lee and co-workers [39], building their homology model of rTRPV1 based on the voltage-dependent shaker family K<sup>+</sup> channel (PDB: 2R9R). The capsaicin bound to their model shared a similar pose with our results.

Figure 1 shows the refined binding pose of compound 1 [24] within TRPV1. By analyzing the TRPV1 binding, we found that the binding pocket was formed by three parts. The upper part of the binding pocket was formed by several hydrophobic residues, including Leu518, Leu547, Phe554, Leu663, and Leu670; the middle consisted of several residues, including Tyr511, Met514, Thr550, and Asn551; while the bottom part was mainly formed by two charged residues, Glu570 and Arg557. These three parts were essential for the binding of ligands (including RTX, capsaicin, and our compound 1) [23, 24]. The docking results showed that the (trifluoromethyl)benzene in compound 1 approached the upper hydrophobic region, the urea group formed the hydrogen bond with Thr550, while the nitro group in the

nitrobenzene formed another hydrogen bond with Arg557. In order to meet these geographical criteria, we selected the diarylurea group as the basic scaffold for our studies.

We performed a substructure search of diarylurea against our previous refined compound library of 15,672 compounds, as shown in Fig. 1. Out of the top 50 hits, 30 of the compounds were available and were purchased from either the NCI or from commercial sources, as shown in Tables I and S1 in the “Supporting Information” section. Among the 30 compounds, compound 5 (partial agonist) yielded an EC<sub>50</sub> value for capsaicin agonism of  $2.84 \pm 0.21 \mu\text{M}$  (Fig. 2, red line,  $55.7 \pm 7.8\%$  agonism). 16 bound to CB2, 15, and 16 (antagonists) yielded  $K_i$  values for capsaicin antagonism of  $0.47 \pm 0.18$  (Fig. 2, blue line,  $100 \pm 0\%$  antagonism at  $30 \mu\text{M}$ ),  $0.49 \pm 0.14$  ( $99.6 \pm 0.4\%$  antagonism at  $30 \mu\text{M}$ ), and  $0.56 \pm 0.16$  ( $100 \pm 0\%$  antagonism at  $30 \mu\text{M}$ )  $\mu\text{M}$ , while compound 14 inhibited [<sup>3</sup>H]RTX binding to hTRPV1 with a  $K_i$  value of  $0.65 \pm 0.26 \mu\text{M}$  (Figure S2). Four compounds showed intermediate antagonistic activity, including compounds 1, 2, 11, and 13, with  $K_i$  values of  $2.57 \pm 0.62$  ( $92.2 \pm 2.7\%$  antagonism at  $30 \mu\text{M}$ ),  $4.52 \pm 0.88$  ( $79.9 \pm 4.9\%$  antagonism at  $30 \mu\text{M}$ ),  $3.7 \pm 1.7$  ( $61 \pm 18\%$  antagonism at  $30 \mu\text{M}$ ), and  $3.7 \pm 1.0$  ( $72 \pm 18\%$  antagonism at  $30 \mu\text{M}$ )  $\mu\text{M}$ , respectively. Compound 4 showed weaker antagonist activity with a  $K_i$  value of  $11.7 \pm 1.3$  ( $64.5 \pm 7.3\%$  antagonism at  $30 \mu\text{M}$ )  $\mu\text{M}$ . Although similar scaffolds (for example, N-substituted naphthylacetamides) have been patented for TRPV1 (WO 2003014064) and CB1 (WO 2006049941), our work reported not only the structure-activity relationship (SAR) of diarylurea analogues and the importance of the nitro/hydroxyl groups/*para*-fluoro but also provided insights into the interactions contributing to the agonist/antagonist balance. Additionally, we presented a novel strategy for simultaneously targeting two or more distinct disease-related proteins for treatment by a single diarylurea molecule. Finally, two compounds, 17 and 18, represented a novel scaffold for antagonism with  $K_i$  values of  $2.15 \pm 0.72$  ( $66 \pm 11\%$  antagonism at  $30 \mu\text{M}$ ) and  $7.0 \pm 2.0$  ( $51.8 \pm 6.6\%$  antagonism at  $30 \mu\text{M}$ )  $\mu\text{M}$ . Four others from Table I, compounds 3, 6, 7, and 10, gave modest inhibition,  $32 \pm 8\%$ ,  $34 \pm 7\%$ ,  $33 \pm 7\%$  and  $35 \pm 5\%$ , respectively, at  $30 \mu\text{M}$ . Similarly, six of the compounds from Table I (compounds 8, 9, and 12) or Table S1 (compounds 23, 25, and 28) gave modest inhibition in the range of 28% to 14% at  $30 \mu\text{M}$ . Finally, the other nine compounds showed <12.5% antagonism at  $30 \mu\text{M}$ . All these results indicated that diarylurea analogues had potential activity on TRPV1. For the 11 compounds for which we had measured  $K_i$  values, we derived from our modeling the predicted  $G$  values for binding. We first docked these 11 compounds into our hTRPV1 model by using the protocol and parameters described above. In SYBYL, the docking score was expressed as  $-\log_{10}(K_d)$  [25]; we predicted the  $G_{\text{predicted}}$  using the equation  $G_{\text{predicted}} = -2.303RT[\text{docking score}]$ , in which  $R$  is the gas constant ( $R = 8.314 \text{ J/mol}\cdot\text{K}$ ) and  $T$  is the absolute temperature ( $T = 273.15^\circ\text{K}$ ). Moreover, we converted the experimental activities ( $K_i$ ) to  $G_{\text{actual}}$  (Figure S3,  $x$ -axis) using the equation  $G_{\text{actual}} = RT \ln K_i$  ( $R = 8.314 \text{ J/mol}\cdot\text{K}$ ;  $T = 273.15 + 37 = 310.15^\circ\text{K}$ , since the  $T$  for the binding was measured at  $37^\circ\text{C}$ ), comparing with the predicted  $G_{\text{predicted}}$  (Figure S3,  $y$ -axis). All the  $G_{\text{predicted}}/G_{\text{actual}}$  data can be found in Figure S3. Our results showed that the  $R$  value is 0.70, indicating that the predicted  $G$  of the binding correlated well with the experimental activities. Moreover, all compounds listed in Tables I and S1 have been validated by “pan assay interference compounds” (PAINS, [www.cbligand.org/PAINS/](http://www.cbligand.org/PAINS/)).



In order to further analyze the influence of R1/R2 (Fig. 1) substitution of diarylurea compounds upon their activities for TRPV1, we performed molecular docking and molecular dynamics simulation (MD) to compare some representative compounds. As shown in Fig. 1, the R1 group was considered to be the group on the diarylurea which was located at the bottom of the binding pocket, close to the charged residues Arg557 and Glu570, while the R2 group was located in the opposite end. For all the compounds discussed below, the binding poses displayed were selected from the cluster of poses obtained based on the frequency and on their docking score. Geographical criteria were used for identifying hydrogen bond, pi-pi interactions, and hydrophobic interactions. We identified a hydrogen bond when the distance between the hydrogen bond donor and acceptor atoms (center of mass) was smaller than 3.5 Å and the angle formed by the hydrogen donor atom, the hydrogen, and the hydrogen bond receptor atom was larger than 135°. For the distances of pi-pi interactions, we measured them based on the centers of mass of the benzene rings. For the hydrophobic interactions, we measured the distance between carbon atom and carbon atom at the hydrophobic residues.

### A Hydrophobic Group in R2 of Diarylurea Small Molecules Confers Enhanced Activity

Compounds 1 and 10 shared almost the same structure but showed quite different activities at TRPV1. The replacement of the *para*-cyano group (compound 10, 35% antagonism at 30 µM) by the *meta*-trifluoromethyl group (compound 1,  $K_i = 2.57 \pm 0.62$  µM, 92.2 ± 2.7% antagonism at 30 µM) significantly increased the activity towards TRPV1. Comparing the detailed interaction modes of compounds 1 and 10 with TRPV1 (Fig. 3), we found many similarities. One of the most important similarities was that the amide and nitro groups in both compounds (compound 1/10) formed hydrogen bonds with residues Thr550 (2.1/3.0 Å) and Arg557 (2.1/ 2.0 Å). These two residues were reported to be critical for forming the hydrogen bond with both agonists and antagonist, including NADA, OLDA, RTX, capsaicin, BCTC,A-425619, AMG9810, SB-366791, capsazepine, and others [24]. However, the *meta*-trifluoromethyl group in compound 1 can insert into a hydrophobic cavity formed from residues Leu518, Leu547, and Leu670 and can make strong hydrophobic interactions (3.7, 3.8, and 4.0 Å) with these residues, contributing to its higher activity. For compound 10, the corresponding *para*-cyano group was directed away from the hydrophobic cavity. Moreover, even if the *para*-cyano group approached this hydrophobic cavity, it cannot form the hydrophobic interactions with these residues. These two factors led to the weaker binding/functional activity of compound 10.

Furthermore, Fig. 4 shows the detailed binding poses of compound 1 ( $2.57 \pm 0.62$  µM) and compound 14 ( $0.47 \pm 0.18$  µM, 100 ± 0% antagonism at 30 µM) with TRPV1. Both the nitro and urea groups of compounds 1 and 14 were found to form hydrogen bonds with Thr550 (2.1 and 2.6 Å) and Arg557 (2.1 and 1.8 Å), and the aromatic ring interacted with two important hydrophobic residues, Leu547 and Leu670. However, the replacement of the *meta*-trifluoromethyl-benzoyl in compound 1 with the 5-hydroxy-1-naphthyl group in compound 14 and shift in the position of the nitro group from the *para*-substituent (compound 1) to the *meta*-substituent (compound 14) improved activity. Moreover, we also found that the replacement of orthochloro with *meta*-fluoro may improve the activity, reflecting among other factors the greater proximity of the *meta*-fluoro to Tyr511 and

Glu570. Last but not least, we found that the 5-hydroxy-1-naphthyl group in R2 inserted more deeply into the hydrophobic cavity with its larger size providing for stronger hydrophobic interactions. The distances between compound 14 and Leu547/Leu670 (3.0 and 2.9 Å) were smaller than those of compound 1 (4.0 and 3.8 Å), indicating that the hydrophobic interactions of compound 14 were stronger. We thus can understand why the introduction of a bulky R2 group enhanced the activity of diarylurea small molecules for TRPV1.

All these results were congruent with the reports [10, 23, 24, 40] that the identified critical hydrophilic and hydrophobic residues, including Tyr511, Leu518, Leu547, Thr550, Asn551, Arg557, and Leu670, were important for compound recognition by TRPV1. Among them, Tyr511, Thr550, Asn551, and Arg557 formed hydrogen bonds with the ligands, while Leu518, Leu547, and Leu670 interacted with the ligands with hydrophobic interactions.

### Important Roles of the Polar/Hydrophilic Group (Nitro and Hydroxyl) in R1 of Diarylurea Inhibitors

Figure 5 shows the detailed binding poses of 16 bound to CB2-16 ( $0.47 \pm 0.18$ ,  $0.49 \pm 0.14$ , and  $0.56 \pm 0.16$  μM), which all were strong antagonists with similar  $K_i$  values in the mid nanomolar range. Each of the three compounds formed at least three hydrogen bonds with several key residues, including Thr550, Asn551, and Arg557.

Although compounds 14 and 15 shared a similar structure, they exhibited opposite binding poses (Fig. 5a, b). The 5-hydroxy-1-naphthyl group of compound 15 pointed down with the hydroxyl group forming a hydrogen bond with Arg557 (2.0 Å). We suggested that the binding poses were reasonable in view of the structures of the two compounds and the properties of the binding pocket in hTRPV1. First, this binding pose was selected based on 43 out of 100 similar poses that were found in our docking results. Moreover, it should be preferable for the charged nitro group in compound 14 to approach and form the hydrogen bonds with the charged regions of TRPV1 (including Arg557, Glu570, and other charged residues), as likewise seen in the docking studies of previous compounds with nitro groups. On the other hand, without a nitro group, the 5-hydroxy-1-naphthyl of compound 15 stretched down and approached Arg557 and Glu570. This binding pose was selected due to the frequency and the docking score; similar binding poses for compound 15 were observed in 57 out of 100 simulations. Moreover, the electronegativity of chloride in compound 15 was smaller than that of hydroxyl. It should be preferable for the 5-hydroxy-1-naphthyl in compound 15 to approach and form hydrophilic interactions with two charged residues (Arg557, Glu570). This rotation of the 5-hydroxy-1-naphthyl group of compound 15 was confirmed by the binding pose of compound 16, in which the meta-hydroxyl group on the benzene ring in compound 16 also formed a hydrogen bond with Arg557. All these results reflect that both the nitro group and the hydroxyl group (polar/hydrophilic group in R1) contributed to the binding affinities of diarylurea inhibitors at TRPV1 and further confirmed that Thr550, Asn551, and Arg557 were important for the recognition of antagonists by TRPV1. These residues have been identified previously as forming hydrophilic interactions with the ligands [23, 41].

## Important Role of the *Para*-Fluoro Group in R2 for Agonism

In the present work, we identified compound 5, which has a *para*-fluoro group in R2, as a partial agonist (Table I and Fig. 2, red line). Compound 4, which has a *meta*-chloro R2 group, was a full antagonist. Except for this modest difference in R2 groups, the structures of compounds 4 and 5 are the same. The binding poses of compounds 4 and 5 are shown in Fig. 6. Their conformations differed by a shift of the carbonyl group in compound 4, which increased the distance and narrowed the angle to form the hydrogen bond with Thr550, thus reducing the strength of the hydrogen bond and its subsequent binding activity. Importantly, the *para*-fluoro benzoyl group of compound 5 extended into the cavity and was closer for interaction with the hydrophobic residues (3.1 Å for Phe543 and 3.5 Å for Leu663). Additionally, the higher electronegativity and smaller atomic radius of the fluoro group could contribute to the formation of a polar interaction or even a hydrogen bond with the hydrogen connected with the carbon on the residues in the cavity. In contrast, the *meta*-chloro benzoyl group in compound 4 pointed out of the cavity and was far away from Phe543 and Leu663. Even if the *meta*-chloro benzoyl group in compound 4 approached these two residues, it cannot form the polar interaction/hydrogen bond with these hydrophobic residues. These results suggest that fluoro replacement in R2, which can generate a hydrogen bond with hydrophobic residues (Phe543 and Leu663) that remains stable during the MD simulations, may convert the antagonist into an agonist (see below). The hydrogen bonds between compound 5 (agonist) and Phe543/Leu663 indicated its potential agonist characteristics. As shown in Figs. 4 and 5, although the hydroxyl in compound 14 also got close to these hydrophobic residues (Phe543 and Leu663), it was identified as an antagonist due to the lack of hydrogen bond or polar interactions.

Recently, Crittenden and colleagues suggested that steric interactions within a binding site were important for determining the type of pharmacological effect of a ligand, i.e., whether a ligand acted as an agonist or an antagonist [41]. In an analogous example, Halim *et al.* [42] showed in docking studies that the methyl group of the (S)-isomer of a GABAergic agonist was well accommodated within the binding site cavity of the “agonist” bound conformation, while the methyl group of the (R)-isomer was sterically interacting with other residues outside the cavity on the GABA receptor [42]. Distinction of the structural requirements for antagonism *versus* agonism has often relied on relatively high-throughput screening to generate initial structural hypotheses and then extensive and iterative biological evaluation of libraries generated by medicinal chemistry. In the present work, to further validate our analysis, we performed a 50 ns MD simulation to evaluate whether the binding with the partial agonist compound 5 induced conformational change of TRPV1, while the antagonist compound 4 did not. From our MD results as shown in Figure S4, we observed that the *para*-fluoro group of compound 5 retained hydrogen bonds with Phe543 and Leu663 (stable at ~3.5 and ~3.6 Å, respectively). These extra hydrogen bonds may contribute to the enlargement of the central pore (see below). However, the *meta*-chloro benzoyl group of compound 4 did not establish such interactions with Phe543 and Leu663 (>5.1 Å). These results were consistent with our docking studies. Figure S5 shows the comparisons of pore radius and conformational changes of hTRPV1 for the binding states with compounds 4 and 5. The average conformation of the hTRPV1 bound with compound 5 during the last 2 ns (48th ns–50th ns) of the simulation was compared with that of the hTRPV1 bound with

compound 4. Figure S5a shows that, in comparison to hTRPV1 bound with compound 4 (antagonist), hTRPV1 bound with compound 5 (partial agonist) displays weak center pore enlargement of the selective filter (~0.2 Å) and a significant enlargement of both the central cavity (~0.7 Å) and the lower gate (1.1 Å). Moreover, Figure S5b shows that a slight outward movement of TM1-4 was observed for hTRPV1 bound with compound 5 (average conformation during the last 2 ns of the simulation), which was also in accordance with our previous report [24] and the agonist-induced cryo-EM structure of TRPV1 [23]: agonist-bound TRPV1 can trigger the movement of transmembrane segments 1–4 and the opening of the central pore (including the selectivity filter and lower gate) to let the ions (for example, Ca<sup>2+</sup>) pass through, while the antagonist blocked the opening of the central pore and the ions cannot pass through.

## DISCUSSION

An emerging concept is the power of designing compounds that can simultaneously interact with more than one therapeutically related target to achieve a synergistic effect. Modeling provides a potent tool for identifying such related targets to guide bioassay and to drive coordinated lead optimization. As discussed below, the diarylurea TRPV1 inhibitors can provide a glimpse of this approach.

### **Polypharmacology of Diarylurea Inhibitors Targeting CB2 for Potential Therapeutics of Neuroinflammation and Osteoporosis**

The cannabinoid receptor 2 (CB2) is an important protein in the endocannabinoid system that has been well recognized for its role in regulating the immune response [43–46]. It has therefore been proposed as an attractive therapeutic target for treating a range of diseases involving inflammation [47] and auto-immune disorders including neurodegenerative diseases and bone loss [48]. The overlap between the therapeutic indications for TRPV1 and CB2 ligands suggests that simultaneously targeting TRPV1 and CB2 may potentially produce a therapeutically useful “dual effect.” Potential applications are in analgesia, drug abuse, cancer, and osteoporosis. For example, CB2 [49] and TRPV1 [50] are potential therapeutic targets for analgesic activity. Recently, Rossi *et al.* [51] highlighted the pivotal role that TRPV1 channels played in bone resorption and suggested a possible cross-talk between TRPV1 and CB2 receptors. They suggested that hybrid compounds acting on both TRPV1 and CB2 receptors but in an opposite manner, with antagonism of TRPV1 and with agonism of CB2, could offer interesting possibilities. 12-Phenylacetyl-ricinoleoyl-vanillamide (phenylacetyl-rivanil, PhAR, IDN5890), an ultra-potent agonist of human vanilloid TRPV1 receptors, has moderate affinity for human cannabinoid CB2 receptors. This compound and its derivatives are dual ligands and have been used for the treatment of inflammation [52]. Here, we reported that the diarylurea analogues showed dual bioactivity for CB2 and hTRPV1. The diarylurea analogues described here and the reported dual compounds are structurally very different.

In the present work, we therefore performed CB2 competition binding assays to measure the binding activities of several of our lead diarylurea TRPV1 antagonists. Interestingly, all three antagonists examined showed binding activity at CB2. Figure 7a shows the binding curve for

compound 15 with a  $K_i$  value of 1.39  $\mu\text{M}$ , while 14 and 16 showed weak binding activity with a  $K_i$  value of 15.9 and 12.2  $\mu\text{M}$  (“Supporting Information” Figure S6). Importantly, both of these three compounds showed no binding affinity at CB1 (data not shown). We then explored the detailed interactions with our CB2 homology model by using molecular docking, as shown in Fig. 7b. Notably, our results showed that compound 15 formed a hydrogen bond with Thr114 (~2.0 Å) and a strong  $\pi$ - $\pi$  interaction with Phe281 (~3.0 Å). Importantly, compound 15 also formed strong hydrophobic interactions with two reported key residues, Trp194 and Phe197. All these results were consistent with the previous studies [26, 53]: Trp194 in TM5 was reported to have an important role in CB2 receptor ligand binding and adenylyl cyclase (AC) activity. Moreover, replacing Phe197 with the corresponding Val282 of CB1 resulted in a 14-fold decrease of WIN55,212-2 affinity to CB2 but had no effect on CP55940, HU-210, or AEA binding [54]. Recently, Phe281 was also reported to form hydrophobic interactions with ligands [26]. On the other hand, the failure of compound 15 to hydrogen bond with Glu181/Ser285 and to form hydrophobic interactions with some other important residues, including Val113, Leu182, Trp258, and Val261, may explain why its affinity was not stronger. Comparing the docking pose of compound 15 at TRPV1 (Fig. 5b) with that at CB2 (Fig. 7b), we suggest that the chemical optimization of the 1-chloro-2-methylbenzene to a bigger hydrophobic group (for example, naphthalene) could enhance both the activity for CB2 (by allowing interaction with Val113, Leu182, and Val261) and for TRPV1 (by enhancing interaction with Phe543, Leu663, and Leu670). We suggest that the 5-methyl-1-naphthyl instead of the 5-hydroxy-1-naphthyl could enhance the selectivity for CB2 due to the hydrophobic properties of CB2’s binding pocket. Importantly, the potential dual activity of diarylurea inhibitors at both CB2 and TRPV1 may imply a potential bi-topic indication of diarylurea inhibitors for treating neuroinflammation and bone resorption diseases, and further SAR may permit optimization of ligands for these twin targets.

### **CXCR2 may be Another Target for Diarylurea Inhibitors with Potential Therapeutics for Neuroinflammation**

The C-X-C chemokine receptor 2, CXCR2, also known as the interleukin 8 receptor beta (IL8RB), is another widely studied target for anti-inflammatory treatment [55]. Upon activation, it triggers the migration of neutrophils to the site of inflammation, a common pathologic pathway in multiple chronic inflammatory disorders including neurodegenerative diseases, chronic obstructive pulmonary disease (COPD), pancreatic cancer, etc. [56, 57]. Although many small molecule inhibitors have been developed for CXCR2, as yet none have been clinically approved. Recently, Dornelles *et al.* [58] explored the role of CXCR2 and TRPV1 for cystitis, and they indicated that the combination of antagonists for these two targets was either synergistic or additive in their therapeutic effect. In this work, we used our in-house tool TargetHunter [59] to predict potential therapeutic targets for the diarylurea compounds. The structure of compound 1 was submitted as a query to the Target Hunter program. Some compounds with higher similarity score (>0.7) were retrieved, including CHEMBL1814524, CHEMBL528275, CHEMBL2069624, CHEMBL224760, and CHEMBL1343296. The additional predicted targets for compound 1, representing the known targets for these similar compounds, include glycogen phosphorylase, HepG2, vascular endothelial growth factor receptor 2, glutamate receptor ionotropic kainate 1, and

*Plasmodium falciparum*. The targets are involved in a wide range of physiological and pharmacological processes, including glucose metabolism and plasma glucose levels, cancer angiogenesis, hepatocellular carcinoma, neurotransmission, and malaria. However, these targets do not have much overlap with therapeutically relevant TRPV1 pathways and will not induce the similar and/or opposite effects that are a prerequisite for a useful dual agent. Interestingly, the query result also yielded a CXCR2 selective inhibitor SB225002, which has a strikingly high similarity (0.75). To further study the potential binding of our compounds with CXCR2, we docked both SB225002 and compound 1 (as an representative compound) into our in-house CXCR2 homology model, which was constructed according to the co-crystal structure of CXCR4 (PDB entry: 3ODU41, resolution: 2.5 Å [60], with 41% identity with CXCR2 [61] as shown in Fig. 8. For validating the 3D model of CXCR2, we selected three candidate models to perform the prescreen with the data set of 1000 compounds, which included ten known active compounds. The binding pocket was predicted using Fast Connolly Type implemented in the MOLCAD module in SYBYL-X 1.3. Some key residues involved in the binding pocket included Lys126, Phe130, Arg184, Cys196, Arg212, Ser217, Phe220, Asn268, Leu271, Asp297, Ile301, and Leu305. These residues were consistent with the results reported by Kruijff and co-workers [62]. The *in silico*-guided mutagenesis studies indicated that the ligand binding cavity for imidazolylpyrimidine compounds in CXCR2 was located between transmembrane (TM) helices 3 (Phe130), 5 (Ser217, Phe220), and 6 (Asn268, Leu271). Figure S7 shows the relationships between the number of hit compounds identified by the bestmodel and the number of compounds screened. All ten known active compounds were among the top 106 compounds.

According to the docking results, these two compounds shared almost the same interactions with the CXCR2 and yielded similar docking scores (8.4 for SB225002 and 8.3 for compound 1), forming hydrogen bonds with Lys126, Arg184, Cys196, and Arg212. Lys126<sup>3,32</sup> in TM3 has been shown to play a key role in CXCR2, and this residue is essential for the recognition of ligands in GPCR [63, 64]. Arg184/Cys196 in extracellular loop 2 (ECL2) and Arg212 in TM5 were also important for the recognition of small molecules by CXCR2 [65]. All these predictions indicated that our docking results were reasonable, and some diarylurea compounds of TRPV1 (especially compound 1) might target CXCR2 for treating chronic inflammatory diseases with synergistic effect. Future studies will seek to test this predicted interaction.

## CONCLUSIONS

For decades, neuroinflammation has been a major focus in studies of neurodegenerative disease. Numerous studies have indicated that neuroinflammatory processes triggered by immune stimuli such as protein aggregates are closely associated with the progressive functional loss of neurons and neurodegeneration. TRPV1 is a critical component in the regulation of neuroinflammation.

In this paper, we screened numerous compounds with the diarylurea pharmacophore and obtained several hits that were expected to have binding/functional activity with TRPV1. The best compounds in the series, compounds 14–16, had  $K_i$  values within the low nanomolar range. We found that a hydrophobic group in R2 and a nitro/hydroxyl group in



R1 were important for the activities of the compounds as demonstrated by bioassay. Moreover, our results showed that fluoro replacement in R2, which can form a hydrogen bond with hydrophobic residues (Phe543 and Leu663), may convert an antagonist into an agonist. Of particular note, we predicted and were then able to confirm the binding activity of compound 15 at CB2. This result suggests that appropriate diarylureas might achieve synergistic effects by targeting two inflammation-related targets and afford drug-repurposing for other kinds of diseases. Compound 1 was predicted to have an inhibitory effect on CXCR2, which could provide another mechanism for its anti-inflammatory effect. However, the *in vitro* binding assays still need to be carried out to experimentally validate the binding activity of our compounds to CXCR2. Overall, our results suggest a novel strategy to use one compound for different but disease-associated targets for treatment of neuroinflammation and neurodegenerative diseases.

## Supplementary Material

Refer to Web version on PubMed Central for supplementary material.

## Acknowledgments

The project is supported by funding to the Xie Laboratory from the NIH, NIDA (P30 DA035778A1) and NIH (R01 DA025612), and in part by the Intramural Program of the Center for Cancer Research, National Cancer Institute, NIH (Project Z1A BC 005270).

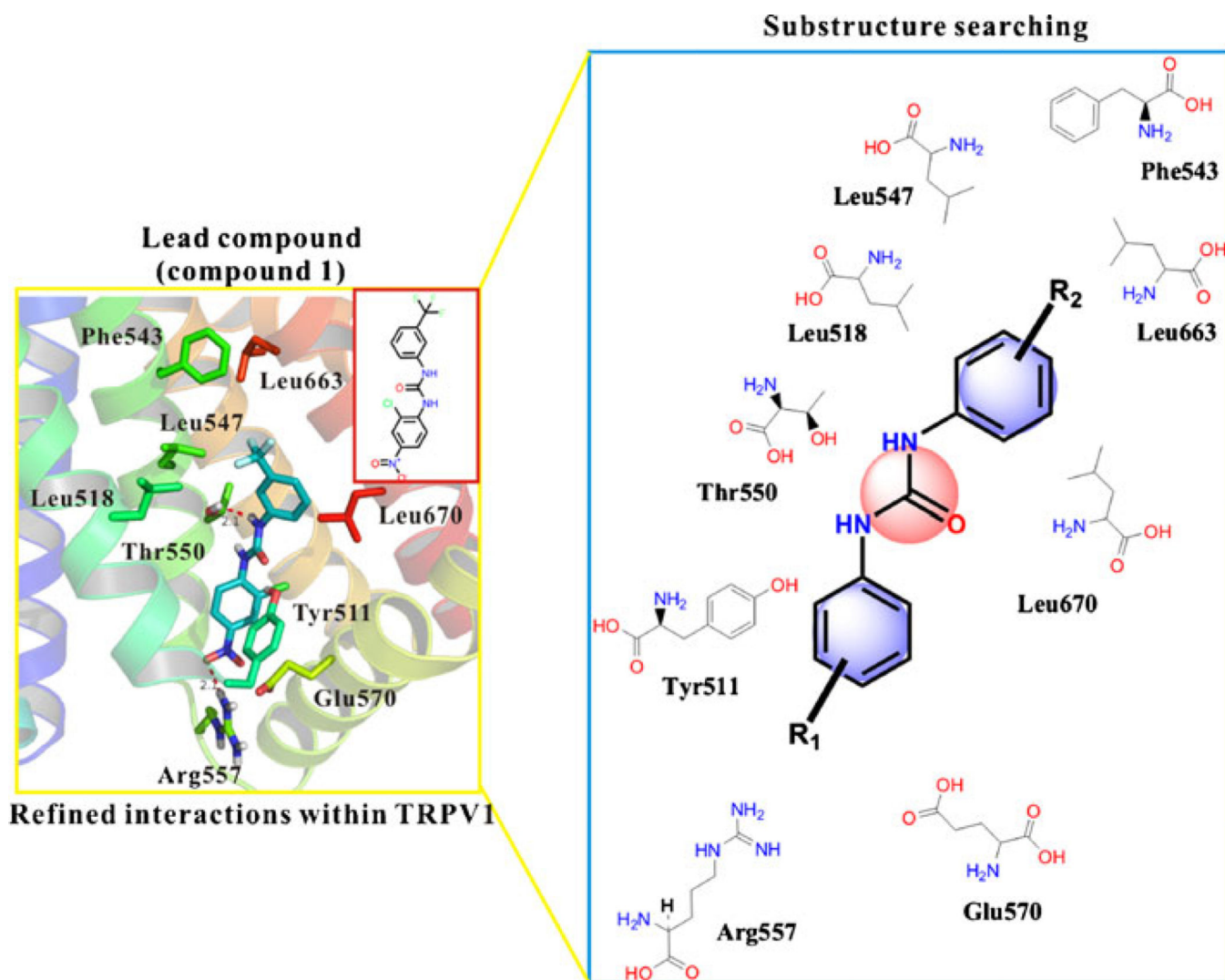
## REFERENCES

1. Gao H-M, Hong J-S. Why neurodegenerative diseases are progressive: uncontrolled inflammation drives disease progression. *Trends Immunol.* 2008; 29(8):357–365. [PubMed: 18599350]
2. Lucas SM, Rothwell NJ, Gibson RM. The role of inflammation in CNS injury and disease. *Br J Pharmacol.* 2006; 147(S1):S232–S240. [PubMed: 16402109]
3. Wyss-Coray T, Mucke L. Inflammation in neurodegenerative disease—a double-edged sword. *Neuron.* 2002; 35(3):419–432. [PubMed: 12165466]
4. de Oliveira ACP, Candelario-Jalil E, Fiebich BL, Santos MdS, Palotás A, Reis HJd. Neuroinflammation and neurodegeneration: pinpointing pathological and pharmacological targets. *BioMed Res Int.* 2015; 2015
5. Craft JM, Watterson DM, Van Eldik LJ. Neuroinflammation: a potential therapeutic target. *Expert Opin Ther Tar.* 2005; 9(5):887–900.
6. Minghetti L. Role of inflammation in neurodegenerative diseases. *Curr Opin Neurol.* 2005; 18(3): 315–321. [PubMed: 15891419]
7. Tansey MG, McCoy MK, Frank-Cannon TC. Neuroinflammatory mechanisms in Parkinson's disease: potential environmental triggers, pathways, and targets for early therapeutic intervention. *Exp Neurol.* 2007; 208(1):1–25. [PubMed: 17720159]
8. Eikelenboom P, Van Gool W. Neuroinflammatory perspectives on the two faces of Alzheimer's disease. *J Neural Transm.* 2004; 111(3):281–294. [PubMed: 14991455]
9. Lukiw WJ, Bazan NG. Neuroinflammatory signaling upregulation in Alzheimer's disease. *Neurochem Res.* 2000; 25(9-10):1173–1184. [PubMed: 11059791]
10. Kim MS, Ki Y, Ahn SY, Yoon S, Kim S-E, Park H-G, et al. Asymmetric synthesis and receptor activity of chiral simplified resiniferatoxin (sRTX) analogues as transient receptor potential vanilloid 1 (TRPV1) ligands. *Bioorg Med Chem Lett.* 2014; 24(1):382–385. [PubMed: 24321344]
11. Macalino SJY, Gosu V, Hong S, Choi S. Role of computer-aided drug design in modern drug discovery. *Arch Pharm Res.* 2015:1–16.

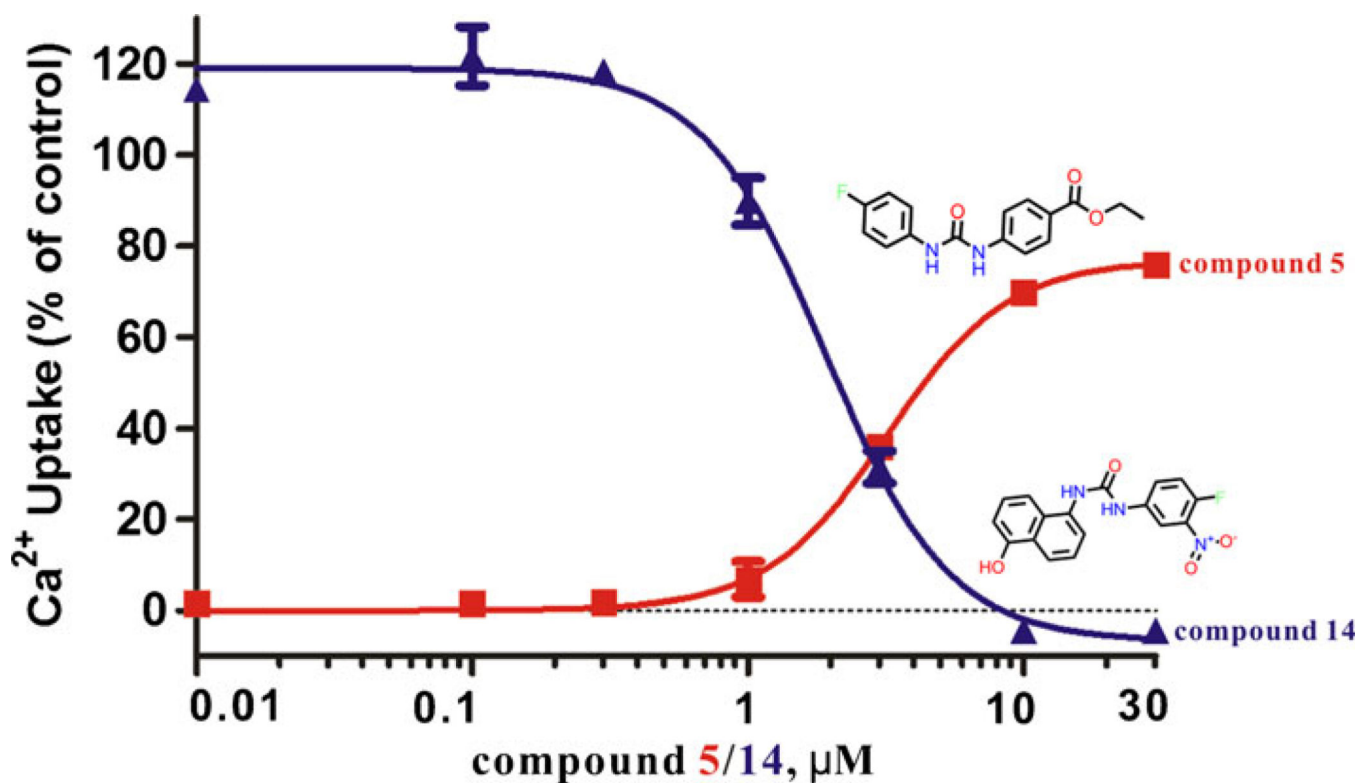
12. Gomtsyan A, McDonald HA, Schmidt RG, Daanen JF, Voight EA, Segreti JA, et al. TRPV1 ligands with hyperthermic, hypothermic and no temperature effects in rats. *Temperature*. 2015; 2:297–301. (just-accepted).
13. Zhang F, Krepiy D, Bae C, Moiseenkova-Bell V, Hanson S, Gorshkova I, et al. Lipid-mediated interaction of double-knot toxin with TRPV1 channels. *Biophys J*. 2014; 106(2):336a.
14. Jiang W, Li W, Hong Y, Wang S, Fang B. Cloning, expression, mutagenesis library construction of glycerol dehydratase, and binding mode simulation of its reactivase with ligands. *Appl Biochem Biotech*. 2015:1–14.
15. Basbaum AI, Bautista DM, Scherrer G, Julius D. Cellular and molecular mechanisms of pain. *Cell*. 2009; 139(2):267–284. [PubMed: 19837031]
16. Khairatkar-Joshi N, Szallasi A. TRPV1 antagonists: the challenges for therapeutic targeting. *Trends Mol Med*. 2009; 15(1):14–22. [PubMed: 19097938]
17. Tominaga M, Caterina MJ, Malmberg AB, Rosen TA, Gilbert H, Skinner K, et al. The cloned capsaicin receptor integrates multiple pain-producing stimuli. *Neuron*. 1998; 21(3):531–543. [PubMed: 9768840]
18. Morgese MG, Cassano T, Cuomo V, Giuffrida A. Anti-dyskinetic effects of cannabinoids in a rat model of Parkinson's disease: role of CB 1 and TRPV1 receptors. *Exp Neurol*. 2007; 208(1):110–119. [PubMed: 17900568]
19. Yamamoto S, Wajima T, Hara Y, Nishida M, Mori Y. Transient receptor potential channels in Alzheimer's disease. *BBA-Mol Basis Dis*. 2007; 1772(8):958–967.
20. Gibson HE, Edwards JG, Page RS, Van Hook MJ, Kauer JA. TRPV1 channels mediate long-term depression at synapses on hippocampal interneurons. *Neuron*. 2008; 57(5):746–759. [PubMed: 18341994]
21. Di Marzo V, Gobbi G, Szallasi A. Brain TRPV1: a depressing TR (i) P down memory lane? *Trends Pharmacol Sci*. 2008; 29(12):594–600. [PubMed: 18947889]
22. Kim SR, Lee DY, Chung ES, Oh UT, Kim SU, Jin BK. Transient receptor potential vanilloid subtype 1 mediates cell death of mesencephalic dopaminergic neurons *in vivo* and *in vitro*. *J Neurosci*. 2005; 25(3):662–671. [PubMed: 15659603]
23. Cao E, Liao M, Cheng Y, Julius D. TRPV1 structures in distinct conformations reveal activation mechanisms. *Nature*. 2013; 504(7478):113–118. [PubMed: 24305161]
24. Feng Z, Pearce LV, Xu X, Yang X, Yang P, Blumberg PM, et al. Structural insight into tetrameric hTRPV1 from homology modeling, molecular docking, molecular dynamics simulation, virtual screening, and bioassay validations. *J Chem Inf Model*. 2015; 55(3):572–588. [PubMed: 25642729]
25. Jain AN. Scoring noncovalent protein-ligand interactions: a continuous differentiable function tuned to compute binding affinities. *J Comput Aided-Mol Des*. 1996; 10(5):427–440. [PubMed: 8951652]
26. Feng Z, Alqarni MH, Yang P, Tong Q, Chowdhury A, Wang L, et al. Modeling, molecular dynamics simulation, and mutation validation for structure of cannabinoid receptor 2 based on known crystal structures of GPCRs. *J Chem Inf Model*. 2014; 54(9):2483–2499. [PubMed: 25141027]
27. Pedretti A, Villa L, Vistoli G. VEGA: a versatile program to convert, handle and visualize molecular structure on Windows-based PCs. *J Mol Graph Model*. 2002; 21(1):47–49. [PubMed: 12413030]
28. Søndergaard CR, Olsson MH, Rostkowski M, Jensen JH. Improved treatment of ligands and coupling effects in empirical calculation and rationalization of pKa values. *J Chem Theory Comput*. 2011; 7(7):2284–2295. [PubMed: 26606496]
29. Hsin J, Arkhipov A, Yin Y, Stone JE, Schulten K. Using VMD: an introductory tutorial. *Curr Protoc Bioinform*. 2008:5.7. 1–5.7. 48.
30. Jorgensen WL, Chandrasekhar J, Madura JD, Impey RW, Klein ML. Comparison of simple potential functions for simulating liquid water. *J Chem Phys*. 1983; 79:926.
31. Kalé L, Skeel R, Bhandarkar M, Brunner R, Gursoy A, Krawetz N, et al. NAMD2: greater scalability for parallel molecular dynamics. *J Comput Phys*. 1999; 151(1):283–312.

32. Karplus M. CHARMM: a program for macromolecular energy, minimization, and dynamics calculations. *J Comput Chem.* 1983; 4:187217.
33. Essmann U, Perera L, Berkowitz ML, Darden T, Lee H, Pedersen LG. A smooth particle mesh Ewald method. *J Chem Phys.* 1995; 103(19):8577–8593.
34. van Veghel D, Cleynhens J, Pearce LV, Blumberg PM, Van Laere K, Verbruggen A, et al. Synthesis and biological evaluation of [<sup>11</sup>C] SB366791: a new PET-radioligand for *in vivo* imaging of the TRPV1 receptor. *Nucl Med Biol.* 2013; 40(1):141–147. [PubMed: 23141549]
35. Chang Y, Prusoff WH. Relationship between the inhibition constant (K<sub>i</sub>) and the concentration of inhibitor which causes 50 per cent inhibition (IC<sub>50</sub>) of an enzymatic reaction. *Biochem Pharmacol.* 1973; 22(23):3099–3108. [PubMed: 4202581]
36. Yang P, Myint K-Z, Tong Q, Feng R, Cao H, Almehizia AA, et al. Lead discovery, chemistry optimization, and biological evaluation studies of novel biamide derivatives as CB2 receptor inverse agonists and osteoclast inhibitors. *J Med Chem.* 2012; 55(22):9973–9987. [PubMed: 23072339]
37. Gertsch J, Leonti M, Raduner S, Racz I, Chen J-Z, Xie X-Q, et al. Beta-caryophyllene is a dietary cannabinoid. *Proc Natl Acad Sci U S A.* 2008; 105(26):9099–9104. [PubMed: 18574142]
38. Zhang Y, Xie Z, Wang L, Schreiter B, Lazo JS, Gertsch J, et al. Mutagenesis and computer modeling studies of a GPCR conserved residue W5. 43 (194) in ligand recognition and signal transduction for CB2 receptor. *Int Immunopharmacol.* 2011; 11(9):1303–1310. [PubMed: 21539938]
39. Lee JH, Lee Y, Ryu H, Kang DW, Lee J, Lazar J, et al. Structural insights into transient receptor potential vanilloid type 1 (TRPV1) from homology modeling, flexible docking, and mutational studies. *J Comput-Aid Mol Des.* 2011; 25(4):317–327.
40. Liao M, Cao E, Julius D, Cheng Y. Structure of the TRPV1 ion channel determined by electron cryo-microscopy. *Nature.* 2013; 504(7478):107–112. [PubMed: 24305160]
41. Crittenden DL, Park A, Qiu J, Silverman RB, Duke RK, Johnston GA, et al. Enantiomers of cis-constrained and flexible 2-substituted GABA analogues exert opposite effects at recombinant GABA C receptors. *Bioorg Med Chem.* 2006; 14(2):447–455. [PubMed: 16183289]
42. Abdel-Halim H, Hanrahan JR, Hibbs DE, Johnston GA, Chebib M. A molecular basis for agonist and antagonist actions at GABAC receptors. *Chem Biol Drug Des.* 2008; 71(4):306–327. [PubMed: 18312293]
43. Yang P, Wang L, Feng R, Almehizia AA, Tong Q, Myint K-Z, et al. Novel triaryl sulfonamide derivatives as selective cannabinoid receptor 2 inverse agonists and osteoclast inhibitors: discovery, optimization, and biological evaluation. *J Med Chem.* 2013; 56(5):2045–2058. [PubMed: 23406429]
44. Chen J-Z, Wang J, Xie X-Q. GPCR structure-based virtual screening approach for CB2 antagonist search. *J Chem Inf Model.* 2007; 47(4):1626–1637. [PubMed: 17580929]
45. Singh J, Lynch D, Grossfield A, Leioatts N, Pitman M, Reggio P. Activation of inhibitory G protein catalyzed by GPCR: molecular dynamics simulations of the activated cannabinoid CB2 receptor/Gαi 1β1γ2 protein complex. *Biophys J.* 2014; 106(2):717a.
46. Mnpotra JS, Qiao Z, Cai J, Lynch DL, Grossfield A, Leioatts N, et al. Structural basis of G protein-coupled receptor-Gi protein interaction : formation of the cannabinoid CB2 receptor-Gi protein complex. *J Biol Chem.* 2014; 289(29):20259–20272. [PubMed: 24855641]
47. Ashton JC, Glass M. The cannabinoid CB2 receptor as a target for inflammation-dependent neurodegeneration. *Curr Neuropharmacol.* 2007; 5(2):73. [PubMed: 18615177]
48. Karsak M, Cohen-Solal M, Freudenberg J, Ostertag A, Morieux C, Kornak U, et al. Cannabinoid receptor type 2 gene is associated with human osteoporosis. *Hum Mol Genet.* 2005; 14(22):3389–3396. [PubMed: 16204352]
49. Hsieh GC, Pai M, Chandran P, Hooker BA, Zhu CZ, Salyers AK, et al. Central and peripheral sites of action for CB2 receptor mediated analgesic activity in chronic inflammatory and neuropathic pain models in rats. *Br J Pharmacol.* 2011; 162(2):428–440. [PubMed: 20880025]
50. Szallasi A, Cruz F, Geppetti P. TRPV1: a therapeutic target for novel analgesic drugs? *Trends Mol Med.* 2006; 12(11):545–554. [PubMed: 16996800]

51. Rossi F, Bellini G, Torella M, Tortora C, Manzo I, Giordano C, et al. The genetic ablation or pharmacological inhibition of TRPV1 signalling is beneficial for the restoration of quiescent osteoclast activity in ovariectomized mice. *Br J Pharmacol.* 2014; 171(10):2621–2630. [PubMed: 24308803]
52. Appendino G, Cascio MG, Bacchiega S, Moriello AS, Minassi A, Thomas A, et al. First “hybrid” ligands of vanilloid TRPV1 and cannabinoid CB 2 receptors and non-polyunsaturated fatty acid-derived CB 2-selective ligands. *FEBS Lett.* 2006; 580(2):568–574. [PubMed: 16406364]
53. Alqarni M, Myint KZ, Tong Q, Yang P, Bartlow P, Wang L, et al. Examining the critical roles of human CB2 receptor residues Valine 3.32 (113) and Leucine 5.41 (192) in ligand recognition and downstream signaling activities. *Biochem Bioph Res Co.* 2014; 452(3):334–339.
54. Song Z-H, Slowey C-A, Hurst DP, Reggio PH. The difference between the CB1 and CB2 cannabinoid receptors at position 5.46 is crucial for the selectivity of WIN55212-2 for CB2. *Mol Pharm.* 1999; 56(4):834–840.
55. Hertzner KM, Donald GW, Hines OJ. CXCR2: a target for pancreatic cancer treatment? *Expert Opin Ther Tar.* 2013; 17(6):667–680.
56. Chapman R, Phillips J, Hipkin R, Curran A, Lundell D, Fine J. CXCR2 antagonists for the treatment of pulmonary disease. *Pharmacol Ther.* 2009; 121(1):55–68. [PubMed: 19026683]
57. Ryu JK, Cho T, Choi HB, Jantarantotai N, McLarnon JG. Pharmacological antagonism of interleukin-8 receptor CXCR2 inhibits inflammatory reactivity and is neuroprotective in an animal model of Alzheimer’s disease. *J Neuroinflamm.* 2015; 12(1):144.
58. Dornelles FN, Andrade EL, Campos MM, Calixto JB. Role of CXCR2 and TRPV1 in functional, inflammatory and behavioural changes in the rat model of cyclophosphamide-induced haemorrhagic cystitis. *Br J Pharmacol.* 2014; 171(2):452–467. [PubMed: 24117268]
59. Wang L, Ma C, Wipf P, Liu H, Su W, Xie X-Q. TargetHunter: an in silico target identification tool for predicting therapeutic potential of small organic molecules based on chemogenomic database. *AAPS J.* 2013; 15(2):395–406. [PubMed: 23292636]
60. Wu B, Chien EY, Mol CD, Fenalti G, Liu W, Katritch V, et al. Structures of the CXCR4 chemokine GPCR with small-molecule and cyclic peptide antagonists. *Science.* 2010; 330(6007):1066–1071. [PubMed: 20929726]
61. Horn F, Weare J, Beukers MW, Hörsch S, Bairoch A, Chen W, et al. GPCRDB: an information system for G protein-coupled receptors. *Nucleic Acids Res.* 1998; 26(1):275–279. [PubMed: 9399852]
62. de Kruijf P, Lim HD, Roumen L, Renjaän VA, Zhao J, Webb ML, et al. Identification of a novel allosteric binding site in the CXCR2 chemokine receptor. *Mol Pharm.* 2011; 80(6):1108–1118.
63. Bertini R, Barcelos L, Beccari A, Cavalieri B, Moriconi A, Bizzarri C, et al. Receptor binding mode and pharmacological characterization of a potent and selective dual CXCR1/CXCR2 non-competitive allosteric inhibitor. *Br J Pharmacol.* 2012; 165(2):436–454. [PubMed: 21718305]
64. Moriconi A, Cesta MC, Cervellera MN, Aramini A, Coniglio S, Colagioia S, et al. Design of noncompetitive interleukin-8 inhibitors acting on CXCR1 and CXCR2. *J Med Chem.* 2007; 50(17):3984–4002. [PubMed: 17665889]
65. Sensi C, Daniele S, Parravicini C, Zappelli E, Russo V, Trincavelli ML, et al. Oxysterols act as promiscuous ligands of class-A GPCRs: in silico molecular modeling and *in vitro* validation. *Cell Signal.* 2014; 26(12):2614–2620. [PubMed: 25152366]



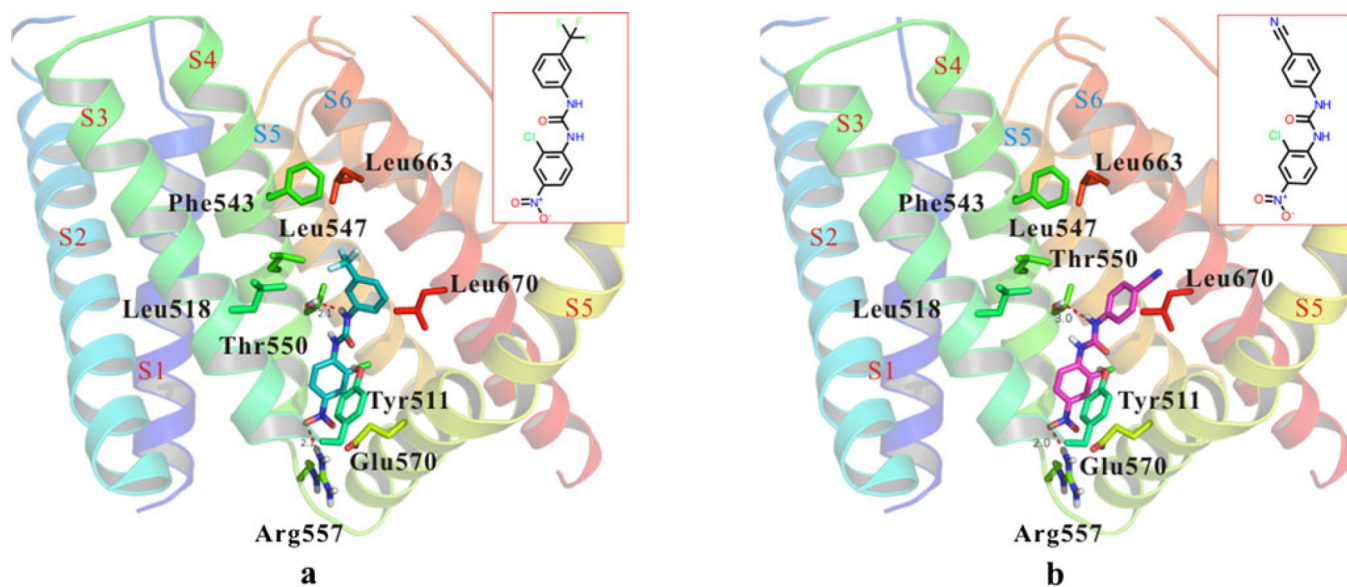
**Fig. 1.** Substructure search of diarylurea small molecules (derived from compound 1) against the refined compound library of 15,672 compounds for TRPV1



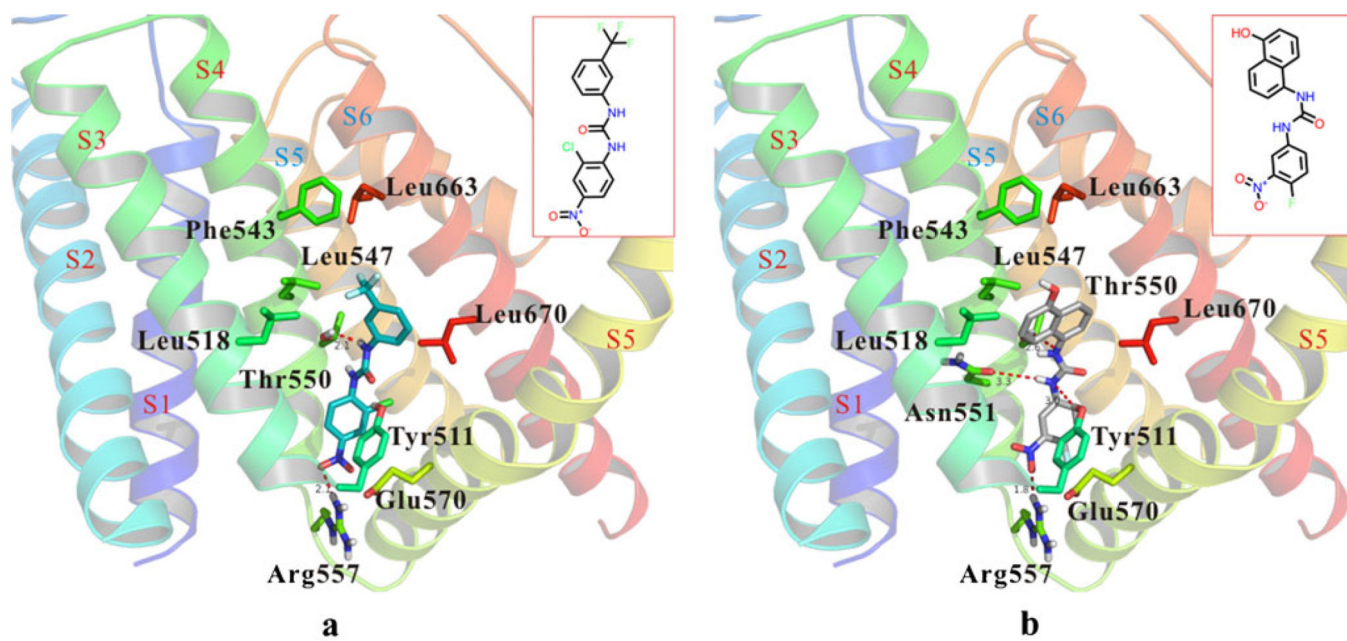
**Fig. 2.**

Chemical structures and activity values of compounds 5 and 14. Compound 5 (partial agonist) yielded an  $\text{EC}_{50}$  value for capsaicin agonism of  $2.84 \pm 0.21 \mu\text{M}$  and maximal stimulation  $55.7 \pm 7.8\%$  of that by 3000 nM capsaicin (Fig. 2, *red line*). Compound 14 (antagonist) yielded a  $K_i$  value for capsaicin antagonism of  $0.47 \pm 0.18 \mu\text{M}$  (Fig. 2, *blue line*) and inhibited [ $^3\text{H}$ ]RTX binding to hTRPV1 with a  $K_i$  value of  $0.65 \pm 0.26 \mu\text{M}$  (Figure S1)

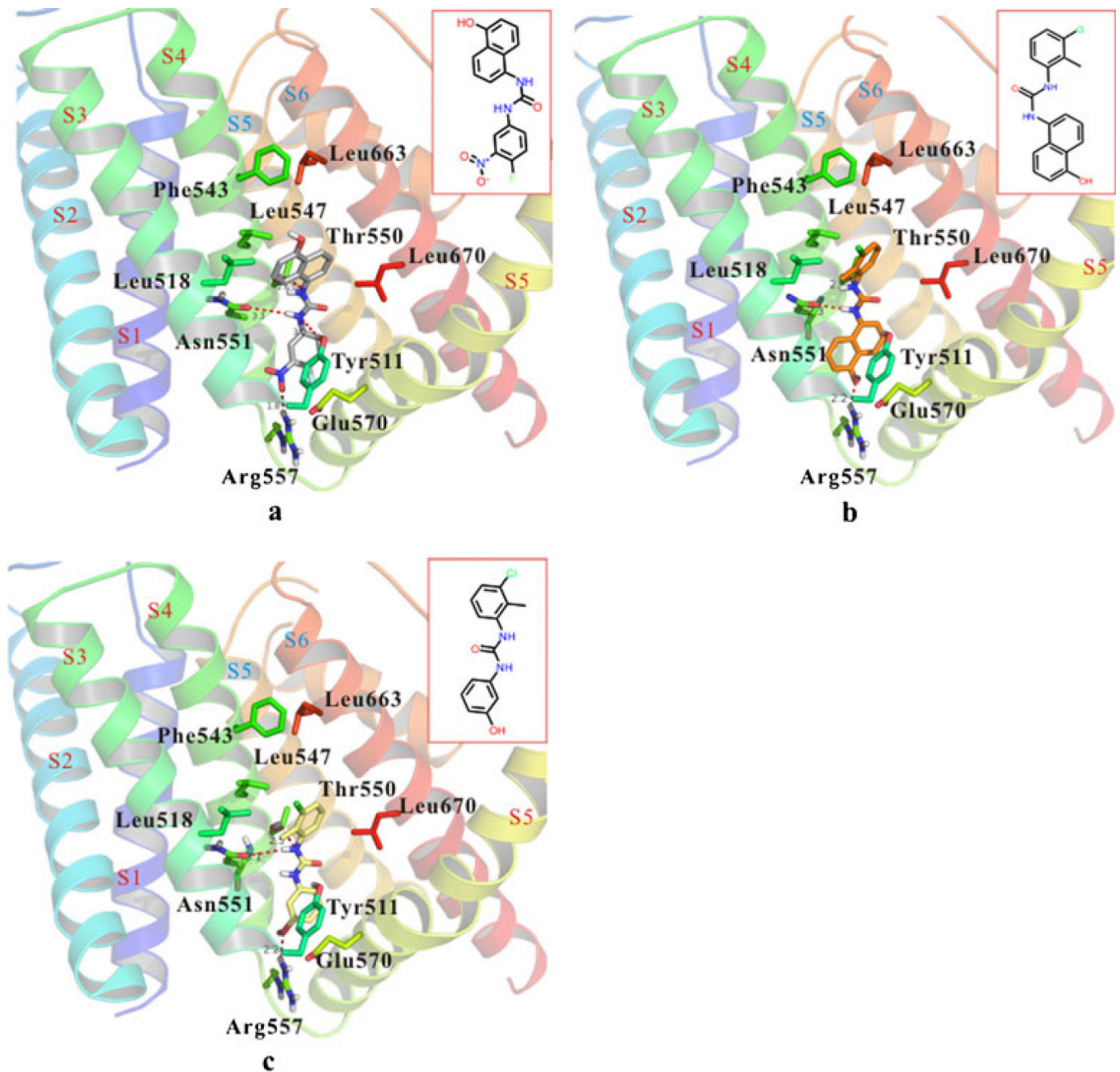




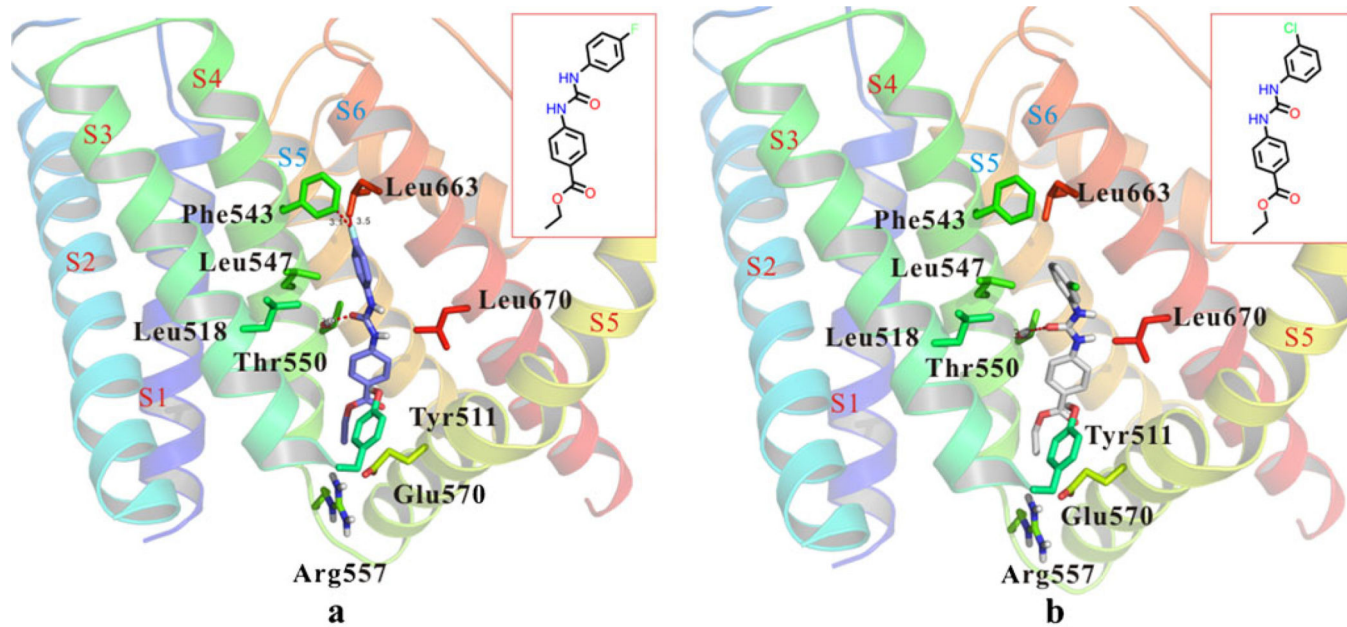
**Fig. 3.** Comparison of compound 1 with compound 10 shows that the *para*-cyano replacement of a *meta*-trifluoromethyl R2 group affected the activity of the compounds at hTRPV1. **a** The detailed binding pose of compound 1 at TRPV1 ( $K_i$ :  $2.57 \pm 0.62 \mu\text{M}$ ). **b** The detailed binding pose of compound 10 at hTRPV1 ( $35 \pm 5\%$  inhibition at  $30 \mu\text{M}$ )



**Fig. 4.** Comparison of compound 1 with compound 14 shows that the bulky R2 group replacement enhanced the activity of the ligand at hTRPV1. **a** The detailed binding pose of compound 1 at hTRPV1 ( $K_i 2.57 \pm 0.62 \mu\text{M}$ ). **b** The detailed binding pose of compound 14 at TRPV1 ( $K_i 0.47 \pm 0.18 \mu\text{M}$ )

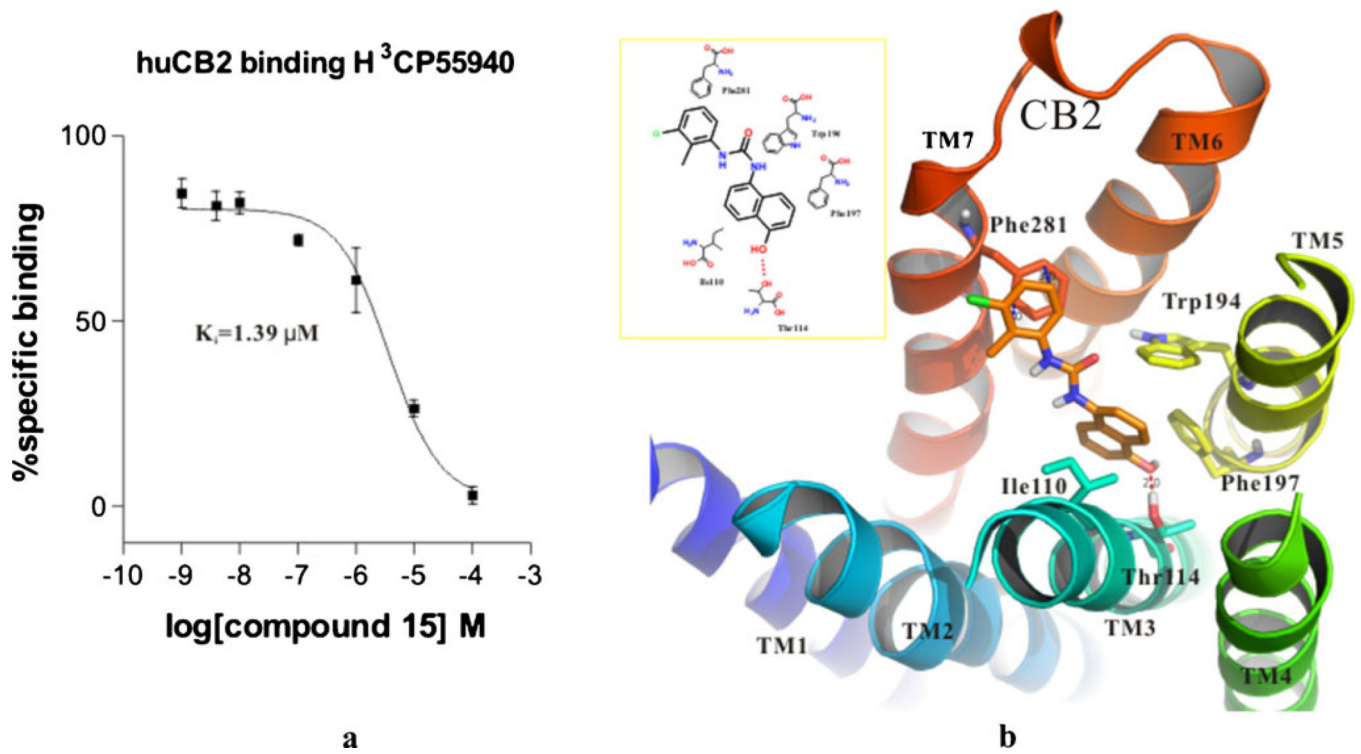


**Fig. 5.** Comparison of compounds 14–16 shows the nitro/hydroxyl group in R1 was important for the activity of inhibitors at hTRPV1. **a** The detailed binding pose of compound 14 at TRPV1 ( $K_i$   $0.47 \pm 0.18 \mu\text{M}$ ). **b** The detailed binding pose of compound 15 at TRPV1 ( $K_i$   $0.49 \pm 0.14 \mu\text{M}$ ). **c** The detailed binding pose of compound 16 at TRPV1 ( $K_i$   $0.56 \pm 0.16 \mu\text{M}$ )

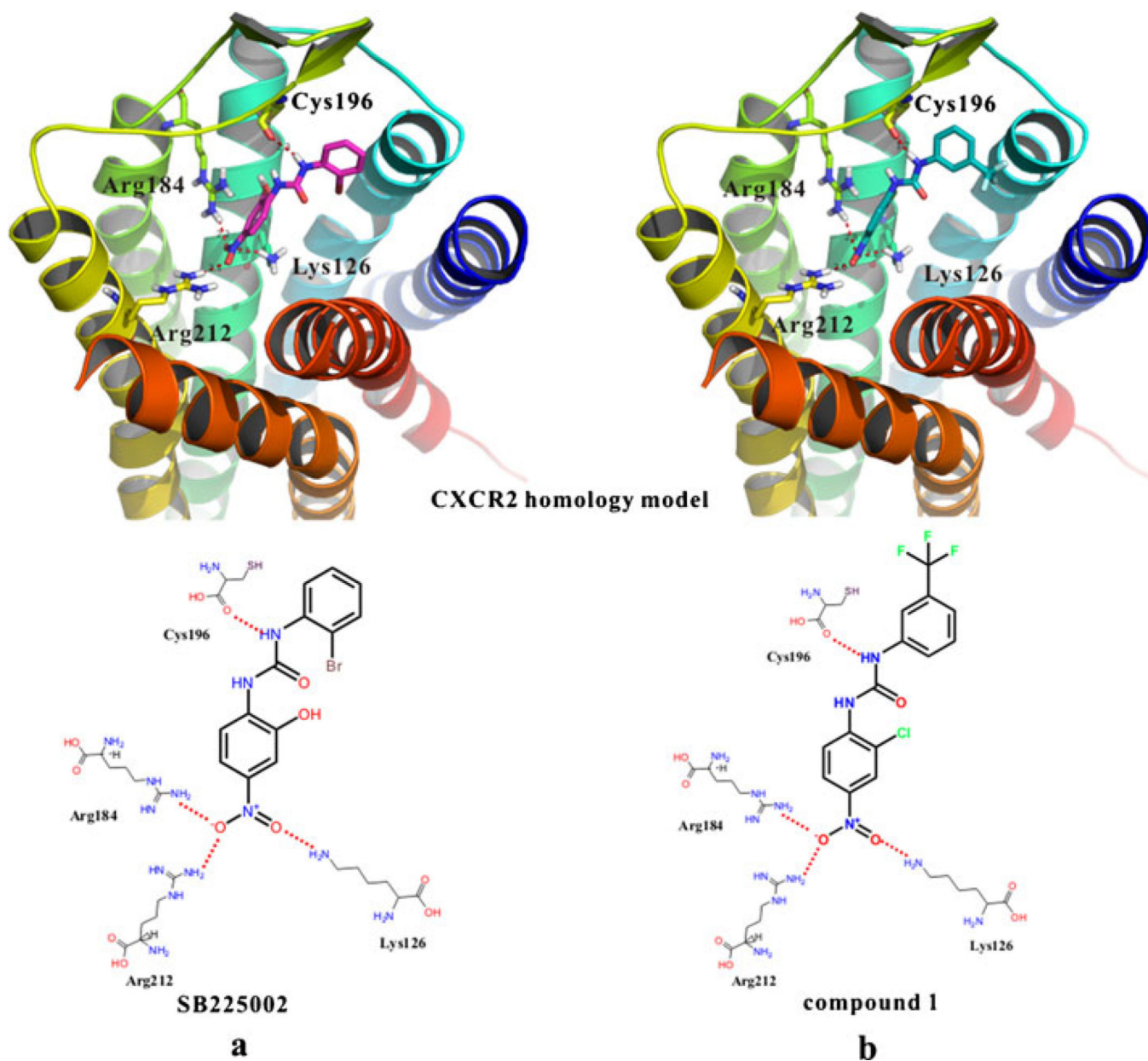


**Fig. 6.** Comparison of the slight different binding modes of compound 5 (partial agonist) and compound 4 (antagonist) at hTRPV1. **a** The detailed binding pose of compound 5 at hTRPV1 ( $EC_{50} 2.84 \pm 0.21 \mu\text{M}$ ). **b** The detailed binding pose of compound 4 at hTRPV1 ( $K_i 11.7 \pm 1.3 \mu\text{M}$ )





**Fig. 7.** Compound 15 of TRPV1 shows potential binding at CB2. **a** The binding curve ( $K_d$  1.39  $\mu\text{M}$ ) of compound 15 at CB2. **b** The detailed binding pose of compound 15 at CB2

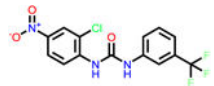
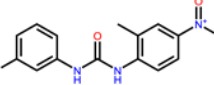
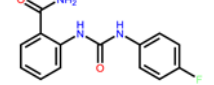
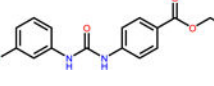
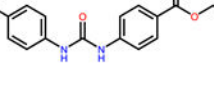
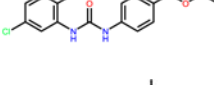
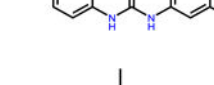
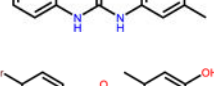
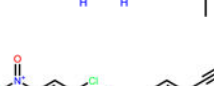

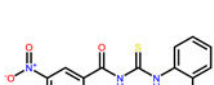



**Fig. 8.** Compound 1 of TRPV1 is predicted to target CXCR2. **a** The potential binding pose of the CXCR2 selective compound SB225002. **b** The potential binding pose of compound 1 at CXCR2. *In vitro* binding assays are still needed to experimentally validate the predicted binding activity of our compounds with CXCR2



Table I

TRPV1 inhibitors

Compound ID	Structure	LogP	MW	$^aK_i$ ( $\mu\text{M}$ ) (or % inhibition at 30 $\mu\text{M}$ )
1		4.09	359.68	$2.57 \pm 0.62$ (92.2 $\pm$ 2.7%)
2		3.04	289.27	$4.52 \pm 0.88$ (79.9 $\pm$ 4.9%)
3		1.58	273.27	$32 \pm 8\%$
4		3.23	318.76	$11.7 \pm 1.3$ (64.5 $\pm$ 7.3%)
b5		2.83	302.31	$2.84 \pm 0.21^b$ (55.7 $\pm$ 7.8% agonism)
6		3.72	332.78	$34 \pm 7\%$
7		2.65	320.77	$33 \pm 7\%$
8		3.03	274.30	$28 \pm 6\%$
9		4.67	363.26	$27 \pm 14\%$
10		2.62	316.70	$35 \pm 5\%$
11		3.93	337.78	$3.7 \pm 1.7$ (61 $\pm$ 18%)
12		3.76	369.32	$23 \pm 12\%$

Compound ID	Structure	LogP	MW	<sup>a</sup> K <sub>i</sub> (μM) (or % inhibition at 30 μM)
13		4.17	326.78	3.7 ± 1.0 (72 ± 18%)
14		3.36	341.30	0.47 ± 0.18 (100 ± 0%)
15		4.17	326.18	0.49 ± 0.14 (99.6 ± 0.40%)
16		3.17	276.72	0.56 ± 0.16 (100 ± 0%)
17		3.23	411.01	2.15 ± 0.72 (66 ± 11%)
18		4.48	317.67	7.0 ± 2.0 (51.8 ± 6.6%)

<sup>a</sup>K<sub>i</sub> values for capsaicin antagonism and % inhibition at 30 μM. For weak compounds, only the inhibition percentage at 30 μM is given

<sup>b</sup>Compound 5 was identified as a partial agonist. The value listed is for agonism. Compounds 17 and 18 were the novel compounds for TRPV1 in the present work. An additional 12 compounds that showed very low activity on TRPV1 can be found in Table S1 in the "Supporting Information" section